JOURNAL OF SOLID STATE CHEMISTRY **123,** 382–390 (1996)
ARTICLE NO. 0193

Electrical Conductivity and Chemical Diffusion Coefficient of Strontium-Doped Lanthanum Manganites

Isamu Yasuda[1] and Masakazu Hishinuma

Fundamental Technology Research Laboratory, Tokyo Gas Co., Ltd., Shibaura, Minato-ku, Tokyo 105, Japan

Received October 23, 1995; in revised form February 23, 1996; accepted February 28, 1996

Electrical conductivity and chemical diffusion coefficient of Sr-doped lanthanum manganites, $La_{1-x}Sr_xMnO_{3\pm\delta}$ (x = 0.05 − 0.20), were measured by the dc four-probe technique and relaxation type experiments where a sudden change of oxygen chemical potential was imposed on the pre-equilibrated sample and the change of electrical conductivity was followed as a function of elapsed time. A defect model is proposed to elucidate the oxygen partial pressure dependence of the measured conductivity and the reported oxygen nonstoichiometry. The transient conductivity behavior after an abrupt change of oxygen partial pressure was successfully described by a diffusion model with consideration of partial control by surface reaction. The determined chemical diffusion coefficients, of the order of 10^{-5} to 10^{-4} cm^2 s^{-1} at 1000°C, increased with decreased oxygen partial pressure due to the thermodynamic enhancement effect. Using the enhancement factor estimated by combination of the proposed defect model and the ambipolar diffusion theory, the oxygen vacancy diffusion coefficients were derived. High vacancy diffusivity comparable to that of Fe- or Co-based perovskites predicts fast oxide ion diffusion under conditions where the manganites show oxygen deficient type nonstoichiometry.

1. INTRODUCTION

Strontium-doped lanthanum manganites, $La_{1-x}Sr_xMnO_{3\pm\delta}$ (abbreviated as LSM), are widely used as air electrodes of solid oxide fuel cells (SOFCs) because of their high electronic conductivity, high catalytic activity for oxygen reduction, and chemical and mechanical compatibility with solid electrolytes based on yttria-stabilized zirconia. To improve the electrode performance, it is of practical importance to understand the mechanism of and to identify the sites for the electrochemical reaction: reduction of gaseous oxygen into oxide ions. The predominance of the process through the triple phase boundary where the solid electrolyte, electrode, and gaseous phase are in direct contact has been postulated in a number of investigations (1–4). The contribution of oxide ion diffusion in the bulk of the electrode material to the electrochemical reaction has also been discussed for large cathodic overpotentials (4–6) and for dense electrodes (7–10). Knowledge of oxygen diffusivity in the electrode material should be useful in examining the possibility of the latter reaction path. Few works, however, have been concerned with oxygen diffusivity in LSM. Belzner *et al.* (11) measured the chemical diffusion coefficient by means of the potential step technique at oxygen partial pressures (Po_2) from 10^{-8} to 0.21 atm. Carter *et al.* (12) studied oxygen tracer diffusivity for limited compositions with relatively high Sr content. The purposes of the present study are to measure the chemical diffusion coefficient of LSM in their oxygen deficient region by means of electrical conductivity relaxation, which has been successfully applied to similar materials based on $LaCrO_3$ (13–15), and to interpret the results in the light of defect chemical equilibrium.

2. EXPERIMENTAL

Powders of four different compositions, x = 0.05, 0.10, 0.15, and 0.20 in $La_{1-x}Sr_xMnO_{3\pm\delta}$, were synthesized by high-temperature solid-state reaction of starting powders of La_2O_3, $SrCO_3$, and $MnCO_3$. Rectangular dense sintered bodies (with relative density of over 98%) of approximately $7 \times 4 \times 25$ mm^3 obtained by uniaxial pressing and sintering of the raw materials at 1400°C for 3 h were used as samples for conductivity measurements. The samples were confirmed by X-ray diffraction analyses to be of single phase with a perovskite-type structure. The electrical conductivity was measured by the dc four-probe technique in a stream of Ar/O_2 or CO/CO_2. The oxygen partial pressure in the atmosphere was monitored by a zirconia sensor placed close to the sample. The chemical diffusion coefficients were determined by analyzing the conductivity relaxation kinetics after an abrupt change in CO/CO_2 mixing ratio. The temperature range covered in this study was 850 to 1000°C. The details of the experimental and analytical procedures were given in a previous paper (14).

[1]To whom all correspondence should be addressed.

0022-4596/96 $18.00

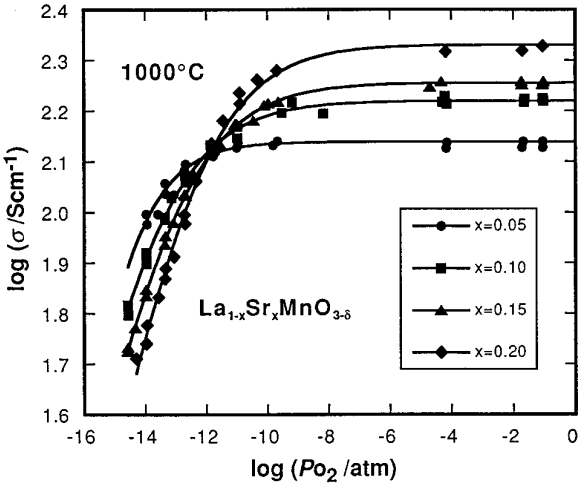

FIG. 1. Electrical conductivity of $La_{1-x}Sr_xMnO_{3\pm\delta}$ (x = 0.05, 0.10, 0.15, and 0.20) at 1000°C as a function of oxygen partial pressure.

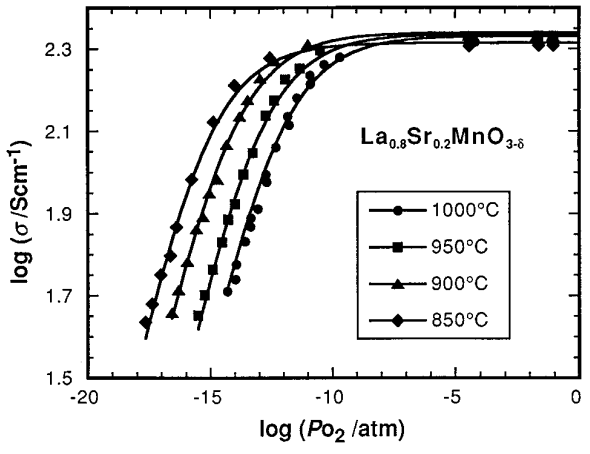

FIG. 2. Electrical conductivity of $La_{0.8}Sr_{0.2}MnO_{3\pm\delta}$ as a function of oxygen partial pressure at four different temperatures: 850°, 900°, 950°, and 1000°C.

3. RESULTS

3.1. Electrical Conductivity

Figure 1 shows the electrical conductivity of the samples with four different compositions at 1000°C as a function of oxygen partial pressure, Po_2. The conductivity takes constant values irrespective of Po_2 at high Po_2 ($>10^{-8}$ atm), while at low Po_2, it decreases exponentially with decreasing Po_2, which is typical behavior for p-type oxide semiconductors. Higher conductivity was recorded for the samples with heavier Sr-doping in the high Po_2 region. In the low Po_2 region, however, the order of conductivity reversed: samples with lower Sr content exhibited higher conductivity at a given Po_2. As will be discussed later in detail, this type of conductivity variation is an indication of transition from electronic to ionic charge compensation; the charge imbalance caused by Sr-doping is compensated for by the formation of Mn^{4+} at high Po_2 (electronic charge compensation) and by the formation of oxygen vacancies at low Po_2 (ionic charge compensation). At Po_2s lower than the leftmost data point for each composition, the conductivity continued to decrease with time and did not reach a stationary value even after 50 h. The Po_2 at which the conductivity starts to fall continuously agrees well with the reported Po_2 for the decomposition of lanthanum manganites (16, 17). This suggests that the sample started to decompose below the critical Po_2.

Figure 2 shows the effect of temperature on the Po_2 dependence of conductivity for $La_{0.8}Sr_{0.2}MnO_{3\pm\delta}$. The same characteristics depicted in Fig. 1—constant conductivity at high Po_2 and exponential decrease at low Po_2—are noted in the results for other temperatures. The Po_2 at which the conductivity starts to decrease with lowering Po_2 increases with raising the temperature. The magnitude of conductivity is slightly higher than the data by Kuo *et al.* (18), the difference of which is believed to come from difference in sample density.

3.2. Chemical Diffusion Coefficient

Typical relaxation data in the form of fractional conductivity change as a function of elapsed time are presented in Fig. 3. When the Po_2 in the atmosphere is changed abruptly, the sample releases its lattice oxygen or incorporates oxygen from the gas phase until it reaches a new thermodynamic equilibrium state. This process comprises two sequential steps: oxygen redox at the surface and bulk diffusion of oxide ions. The effect of the surface reaction

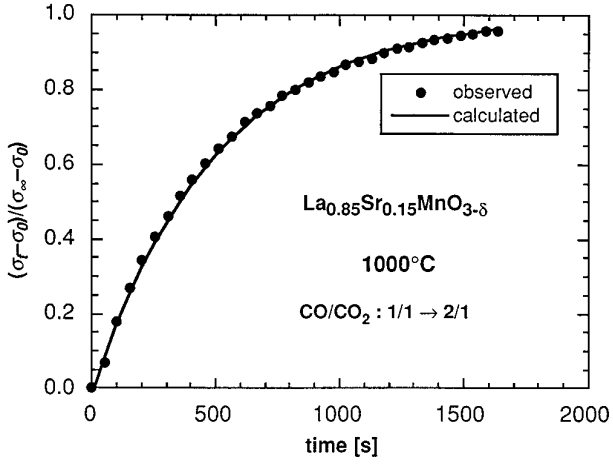

FIG. 3. Fractional change of conductivity as a function of elapsed time after gas switching. The mixing ratio of CO to CO_2 was abruptly changed from 1/1 to 2/1; the oxygen partial pressure in the atmosphere was decreased. Solid curve is the best fit to the theoretical equation (Eq. [4]).

should be considered as the boundary condition for obtaining a solution to Fick's second law. The analytical solution for the plane sheet geometry with consideration of the surface effect was obtained by Crank (19), approximating the surface reaction kinetics as linear with respect to the oxygen concentration at the surface. Here, Crank's solution is expanded to a rectangular geometry of width $2w$, thickness $2h$ and length $2l$, as

$$\frac{M_t}{M_\infty} = 1 - \sum_{i=1}^{\infty}\sum_{m=1}^{\infty}\sum_{n=1}^{\infty} \frac{2L_1^2 \exp(-\beta_i^2 D_{\text{chem}} t/h^2)}{\beta_i^2(\beta_i^2 + L_1^2 + L_1)} \times \frac{2L_2^2 \exp(-\gamma_m^2 D_{\text{chem}} t/w^2)}{\gamma_m^2(\gamma_m^2 + L_2^2 + L_2)} \times \frac{2L_3^2 \exp(-\delta_n^2 D_{\text{chem}} t/l^2)}{\delta_n^2(\delta_n^2 + L_3^2 + L_3)}, \quad [1]$$

where D_{chem} is the chemical diffusion coefficient, t is the diffusion time, and M_t/M_∞ in the left side denotes the ratio of total amount of oxygen diffused at time t to that at time infinity. The dimensionless parameters L_1, L_2, and L_3 are defined using the linear rate constant (α) and the chemical diffusion coefficient as

$$L_1 = h\alpha/D_{\text{chem}} \quad [2a]$$

$$L_2 = w\alpha/D_{\text{chem}} \quad [2b]$$

$$L_3 = l\alpha/D_{\text{chem}}, \quad [2c]$$

which serve as a good measure of the significance of the surface reaction; large and small L's correspond to diffusion-controlled and surface-reaction-controlled processes, respectively. β_n, γ_n, and δ_n are the nth roots of the equations:

$$\beta_n \tan \beta_n = L_1 \quad [3a]$$

$$\gamma_n \tan \gamma_n = L_2 \quad [3b]$$

$$\delta_n \tan \delta_n = L_3 \quad [3c]$$

When the magnitude of the Po_2 change is not very large, the mobility of the charge carrier can be approximated as constant during the course of relaxation; a linear relation can be assumed between the changes of the electrical conductivity and the concentration of the lattice oxygen or the oxygen vacancies (14). This rewrites the left side of Eq. [1] as

$$\frac{\sigma_t - \sigma_0}{\sigma_\infty - \sigma_0} = 1 - \sum_{i=1}^{\infty}\sum_{m=1}^{\infty}\sum_{n=1}^{\infty} \frac{2L_1^2 \exp(-\beta_i^2 D_{\text{chem}} t/h^2)}{\beta_i^2(\beta_i^2 + L_1^2 + L_1)} \times \frac{2L_2^2 \exp(-\gamma_m^2 D_{\text{chem}} t/w^2)}{\gamma_m^2(\gamma_m^2 + L_2^2 + L_2)} \times \frac{2L_3^2 \exp(-\delta_n^2 D_{\text{chem}} t/l^2)}{\delta_n^2(\delta_n^2 + L_3^2 + L_3)}, \quad [4]$$

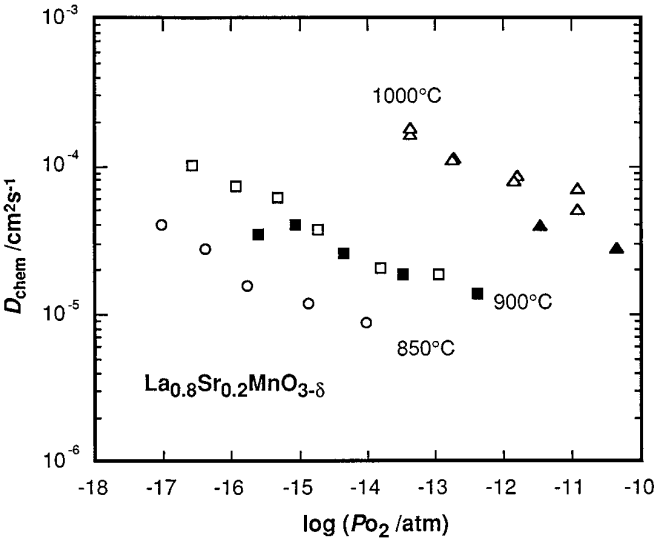

FIG. 4. The effect of temperature on the oxygen partial pressure dependence of the chemical diffusion coefficient of $La_{0.8}Sr_{0.2}MnO_{3\pm\delta}$. Open and closed symbols show the data from reduction and oxidation runs, respectively.

where σ_0, σ_∞, and σ_t denote the apparent conductivity at $t = 0$ (initial), ∞ (after reaching a new equilibrium state), and t (in the course of relaxation).

The solid line in Fig. 3 was drawn by fitting the observed time change of conductivity to the above equation taking α and D_{chem} as fitting parameters. A good fit of the theoretical line to the experimental results is clearly seen, which leads to the conclusion that the conductivity relaxation kinetics is well described by the present model which considers both bulk diffusion and partial control by surface reaction.

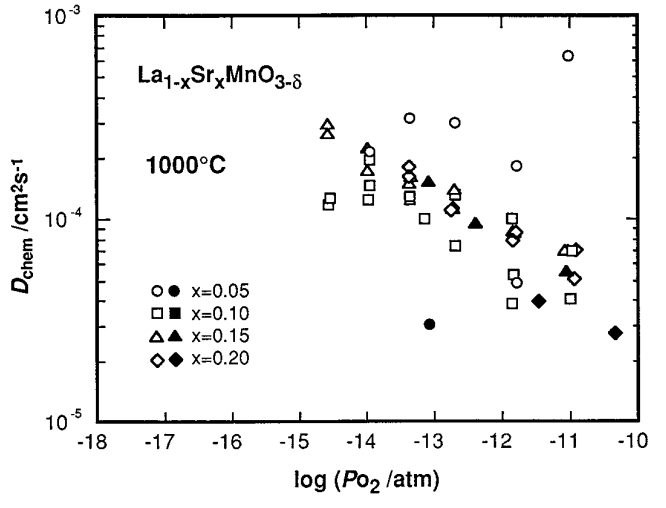

FIG. 5. Chemical diffusion coefficient of $La_{1-x}Sr_xMnO_{3\pm\delta}$ at 1000°C as a function of oxygen partial pressure. Open and closed symbols show the data from reduction and oxidation runs, respectively.

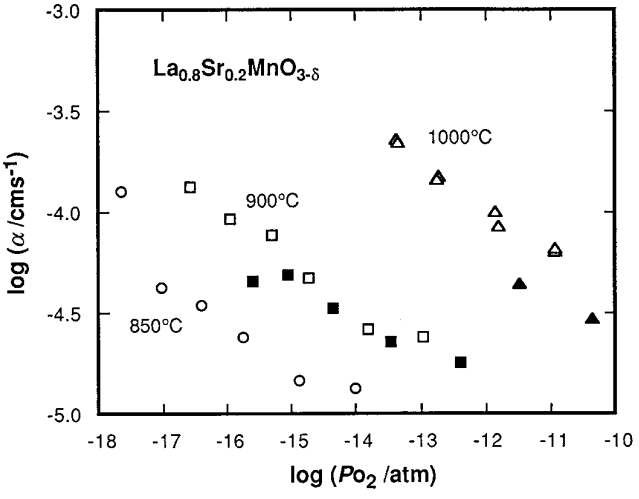

FIG. 6. Surface reaction rate constant of $La_{0.8}Sr_{0.2}MnO_{3\pm\delta}$ as a function of oxygen partial pressure. Open and closed symbols show the data from reduction and oxidation runs, respectively.

The chemical diffusion coefficients thus determined are plotted as a function of Po_2 in Figs. 4 and 5, showing the effect of temperature and composition on the Po_2 dependence. Open and closed symbols in the figures represent the data from reduction and oxidation runs, respectively. From the fact that in the whole Po_2 range the same diffusion coefficients were obtained independent of the sample dimension and direction of Po_2 change, it can be concluded that the true bulk diffusivity was successfully determined by separating the effect of the surface reaction. The value of D_{chem}, of the order of 10^{-5} to 10^{-4} cm^2 s^{-1}, does not strongly depend on the amount of Sr-doping, and it increases with decreased Po_2. Such a Po_2 dependence of D_{chem} is attributable to the so-called thermodynamic enhancement effect, which will be quantitatively discussed later. At a given Po_2, D_{chem} increases as the temperature increases, which can be easily understood from the fact that thermally activated jumps between lattice sites are the elementary steps of the chemical diffusion process.

Figure 6 plots the surface reaction rate constant of $La_{0.8}Sr_{0.2}MnO_{3\pm\delta}$ as a function of Po_2. Similarly to the Po_2 dependence of D_{chem} as shown in the previous graphs, it is seen that the surface reaction rate constant increases from 10^{-5} to 10^{-4} cm/s with decrease of Po_2.

4. DISCUSSION

4.1. Defect Equilibrium in the Oxygen Deficient Region

The chemical diffusion coefficient is closely related to the change of concentration of the mobile defects. Accordingly, the defect equilibrium in the system of interest must be made clear in examining the Po_2 dependence of chemical diffusivity. LSM have been known to show oxygen excess type nonstoichiometry at high Po_2 and oxygen deficient type nonstoichiometry at low Po_2 (18, 20, 21). Because the conductivity relaxation experiments were conducted under conditions corresponding to the oxygen deficient region, a defect chemical analysis will be focused on the oxygen deficient type nonstoichiometry. Three types of defect models are proposed to elucidate the Po_2 dependence of oxygen nonstoichiometry and electrical conductivity.

The first model, MODEL 1, considers Sr'_{La}, $Mn^{\cdot}_{Mn}$, and $V^{\cdot\cdot}_{O}$ as predominant point defects. Hereafter, the Kröger–Vink notation (22) is used to present the point defects. Assuming that the charge imbalance caused by the introduction of an aliovalent impurity, Sr in the present case, is compensated electronically (through oxidation of part of Mn^{3+} ions to Mn^{4+} ions) at relatively high Po_2 and that the ionic contribution (formation of double-positively charged oxygen vacancies at the expense of Mn^{4+}) becomes more significant as Po_2 decreases, the pseudo-chemical reaction between the point defects and oxygen in the gas phase can be expressed as

$$2Mn^{\cdot}_{Mn} + O^{x}_{O} = 2Mn^{x}_{Mn} + V^{\cdot\cdot}_{O} + \frac{1}{2}O_2, \qquad [5]$$

and the equilibrium constant for this reaction is

$$K_5 = \frac{[Mn^{x}_{Mn}]^2[V^{\cdot\cdot}_{O}]P^{1/2}_{O_2}}{[Mn^{\cdot}_{Mn}]^2[O^{x}_{O}]}. \qquad [6]$$

Because the sum of relative charges on point defects over the whole crystal must be zero (the electroneutrality requirement), the following relationship must hold among the concentrations of charged point defects:

$$[Sr'_{La}] = [Mn^{\cdot}_{Mn}] + 2[V^{\cdot\cdot}_{O}]. \qquad [7]$$

Under the present experimental conditions, no species other than oxygen are volatile, from which are derived the site relations

$$[Mn^{\cdot}_{Mn}] + [Mn^{x}_{Mn}] = 1 \qquad [8]$$

$$[V^{\cdot\cdot}_{O}] + [O^{x}_{O}] = 3, \qquad [9]$$

where the concentrations of defects are expressed in terms of mole fractions: moles of defects in one mole LSM. The Po_2- and temperature-dependent variables are $[Mn^{\cdot}_{Mn}]$, $[Mn^{x}_{Mn}]$, $[V^{\cdot\cdot}_{O}]$, and $[O^{x}_{O}]$, which are related to each other through Eqs. [6]–[9]. When the equilibrium constant for the defect reaction, K_5, is known, the concentrations of the four point defects can be calculated for a given condition.

When the concentration of one of the four point defects is available as a function of Po_2, one can determine K_5. This type of defect model has been successfully applied to elucidate nonstoichiometric behavior of acceptor-doped $LaCrO_3$ (23–25).

The second model, MODEL 2, considers the disproportionation of Mn^{3+} into Mn^{2+} and Mn^{4+} (13, 26–28), in addition to the oxygen vacancy formation (Eq. [5]), as

$$2Mn^{x}_{Mn} = Mn^{\cdot}_{Mn} + Mn'_{Mn} \quad [10]$$

$$K_{10} = \frac{[Mn^{\cdot}_{Mn}][Mn'_{Mn}]}{[Mn^{x}_{Mn}]^2}. \quad [11]$$

The electroneutrality condition and site relations are expressed as

$$[Sr'_{La}] + [Mn'_{Mn}] = [Mn^{\cdot}_{Mn}] + 2[V^{\cdot\cdot}_{O}] \quad [12]$$

$$[Mn^{\cdot}_{Mn}] + [Mn^{x}_{Mn}] + [Mn'_{Mn}] = 1 \quad [13]$$

$$[V^{\cdot\cdot}_{O}] + [O^{x}_{O}] = 3. \quad [14]$$

The Po_2 and temperature dependent variables are $[Mn^{\cdot}_{Mn}]$, $[Mn'_{Mn}]$, $[Mn^{x}_{Mn}]$, $[V^{\cdot\cdot}_{O}]$, and $[O^{x}_{O}]$, which are related to each other through Eqs. [6] and [11]–[14]. This type of defect model was proposed by Mizusaki *et al.* (29) to elucidate the defect equilibrium in acceptor-doped $LaFeO_3$. Kuo *et al.* (18) used this model to interpret the Po_2 dependence of oxygen nonstoichiometry and electrical conductivity of LSM.

In the third model, MODEL 3, all divalent manganese ions, $[Mn'_{Mn}]$, generated as a result of the charge disproportionation of Mn^{3+} (Eq. [10]) are assumed to be bound to oxygen vacancies, forming a neutral defect cluster $\langle Mn'_{Mn} - V^{\cdot\cdot}_{O} - Mn'_{Mn}\rangle$, which was proposed by van Roosmalen and Cordfunke (30) in their defect chemical analysis on nondoped $LaMnO_3$. This process can be expressed as

$$2Mn^{x}_{Mn} + O^{x}_{O} = \langle Mn'_{Mn} - V^{\cdot\cdot}_{O} - Mn'_{Mn}\rangle + \frac{1}{2}O_2 \quad [15]$$

$$K_{15} = \frac{[\langle Mn'_{Mn} - V^{\cdot\cdot}_{O} - Mn'_{Mn}\rangle]P^{1/2}_{O_2}}{[Mn^{x}_{Mn}]^2[O^{x}_{O}]}. \quad [16]$$

The following electroneutrality requirement and site relations must hold among the concentrations of point and extended defects:

$$[Sr'_{La}] = [Mn^{\cdot}_{Mn}] + 2[V^{\cdot\cdot}_{O}] \quad [17]$$

$$[Mn^{\cdot}_{Mn}] + [Mn^{x}_{Mn}] + 2[\langle Mn'_{Mn}] - [V^{\cdot\cdot}_{O}] - Mn'_{Mn}\rangle] = 1 \quad [18]$$

$$[V^{\cdot\cdot}_{O}] + [\langle Mn'_{Mn}] - [V^{\cdot\cdot}_{O}] - Mn'_{Mn}\rangle] + [O^{x}_{O}] = 3. \quad [19]$$

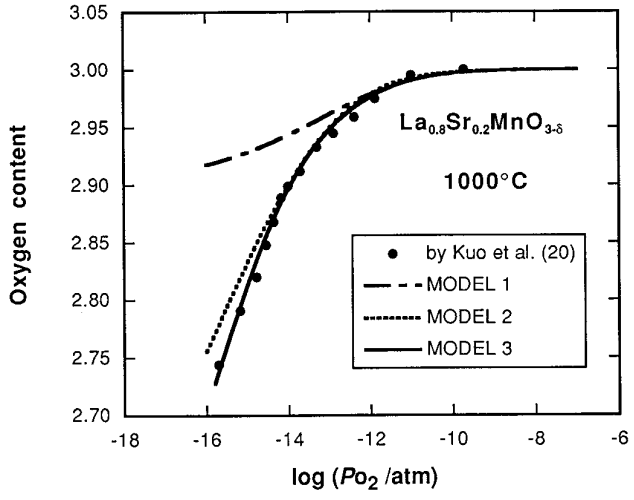

FIG. 7. Oxygen nonstoichiometry of $La_{0.8}Sr_{0.2}MnO_{3\pm\delta}$ at 1000°C. Three types of defect models are fitted to the thermogravimetric data reported by Kuo *et al.* (20).

There are five variable parameters, $[Mn^{\cdot}_{Mn}]$, $[\langle Mn'_{Mn} - V^{\cdot\cdot}_{O} - Mn'_{Mn}\rangle]$, $[Mn^{x}_{Mn}]$, $[V^{\cdot\cdot}_{O}]$, and $[O^{x}_{O}]$, which should simultaneously satisfy five independent equations, Eqs. [6], and [16]–[19].

In the following, the results of theoretical analyses of the experimental data are given for the composition with $x = 0.20$, since the nonstoichiometry data for this composition are available in the literature and this composition is close to that of the practically applied air electrode material for SOFC. The nonstoichiometry data reported by Kuo *et al.* (20) are analyzed based on the three defect models, and the results for $x = 0.20$ are shown in Fig. 7. With the first model, the mole fraction of oxygen vacancy never exceeds the limiting value of 0.1 fixed by the degree of Sr-doping. This prediction is in contradiction to the reported nonstoichiometry data showing that the oxygen content decreases far below the limiting value (2.9). The second and third models both seem to properly describe the nonstoichiometric behavior; the third one shows a better fit to the experimental data.

Using the equilibrium constants for the defect reactions (K_5, K_{10}, and K_{15}) determined to give the smallest differences between the model calculations and the experimental nonstoichiometry data (20), the concentrations of major defects are calculated. The results for MODEL 2 and 3 are shown in terms of mole fractions of defects vs log Po_2 in Fig. 8. The results from MODEL 2 (Fig. 8a) show that at Po_2 lower than about 10^{-14} atm the concentration of Mn'_{Mn} surpasses that of $Mn^{\cdot}_{Mn}$. This leads to the prediction that the sample shows a transition from *p*-type to *n*-type conduction: the electrical conductivity is expected to first decrease, show a minimum, and then start to increase as Po_2 is lowered. But such a behavior is not observed in

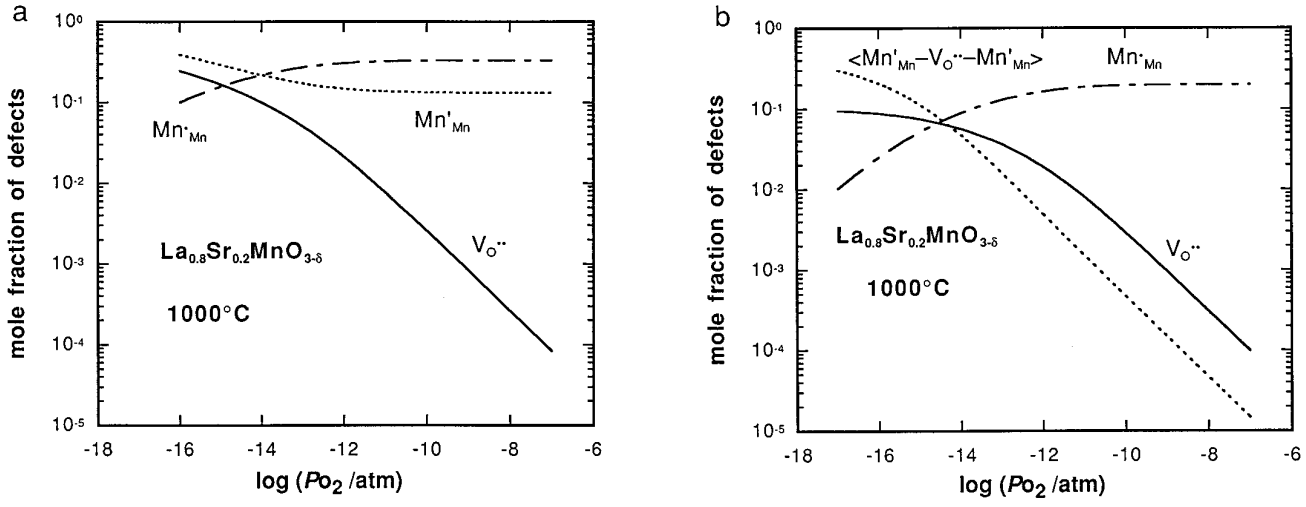

FIG. 8. Mole fractions of point defects in $La_{0.8}Sr_{0.2}MnO_{3\pm\delta}$ at 1000°C as a function of oxygen partial pressure calculated by using MODEL 2 (a) and MODEL 3 (b).

the measured conductivity vs Po_2 relationship previously shown in Figs. 1 and 2. Thus, MODEL 2 has failed to describe the Po_2 dependence of electrical conductivity although it satisfactorily accounts for the nonstoichiometric behavior. On the other hand, with MODEL 3, the electrons are assumed to be strongly bound to the association pairs (i.e., be captured or trapped) and not to contribute to electrical conduction. In this situation, the conductivity is determined exclusively by the concentration of $Mn^{\cdot}_{Mn}$, which is graphically shown in Fig. 9, comparing the Po_2 dependence of the measured conductivity with the calculated hole concentration, $[Mn^{\cdot}_{Mn}]$, as a function of Po_2. Very good agreement can be found between them, from which we can conclude that MODEL 3 successfully elucidates the Po_2 dependence of both oxygen nonstoichiometry and electrical conductivity. Therefore, further discussions of the Po_2 dependence of the chemical diffusion coefficient will be based on this defect model. The two equilibrium constants, K_5 and K_{15}, determined to best fit the reported nonstoichiometry data (20) are listed in Table 1. Both equilibrium constants increase with rising temperature, which indicates that the concentrations of oxygen vacancies and association pairs increase with increasing temperature.

With MODEL 3, as shown in Fig. 8b, it is found that most of the oxygen vacancies are in a free state in the Po_2 range of $-12 < \log Po_2 < -7$, while at rather low Po_2, the concentration of the association pairs surpasses that of free vacancies; more than half of the oxygen vacancies are in a frozen state. Figure 9 also shows the hole mobility calculated from the measured conductivity and the simulated hole concentration. It is seen that the mobility gradually increases as Po_2 decreases. With one or less decade of Po_2 change subject to the samples in the relaxation experiments, the mobility can reasonably be approximated as constant, which justifies the assumption of constant mobility introduced in the derivation of Eq. [4]. The calculated mobility is in the range of 0.39 to 0.50 $cm^2\ V^{-1}\ s^{-1}$, which is higher than the criterion for small polaron hopping conduction ($<0.1\ cm^2\ V^{-1}\ s^{-1}$ [31, 32]).

4.2. Oxygen Partial Pressure Dependence of Chemical Diffusion Coefficient

When the Po_2 is abruptly changed in the conductivity relaxation experiments, the concentration of oxygen vacancies at the sample surface changes and a gradient of oxygen vacancy concentration is established within the sample, which is a driving force for diffusion of oxygen vacancies. The electroneutrality condition requires the simultaneous setup of a concentration gradient of electron

TABLE 1
Equilibrium Constant of the Defect Reactions [5] and [15]

Composition	Temperature [°C]	K_5 [$atm^{1/2}$]	K_{15} [$atm^{1/2}$]
LSM5	1000	9.1×10^{-7}	3.1×10^{-10}
	1100	1.4×10^{-5}	2.9×10^{-9}
	1200	2.6×10^{-5}	2.2×10^{-8}
LSM10	1000	6.0×10^{-8}	6.8×10^{-10}
	1100	1.0×10^{-6}	5.6×10^{-9}
	1200	3.5×10^{-5}	3.8×10^{-8}
LSM20	1000	1.7×10^{-7}	2.4×10^{-9}
	1100	1.7×10^{-9}	6.6×10^{-8}
	1200	3.8×10^{-6}	7.5×10^{-8}

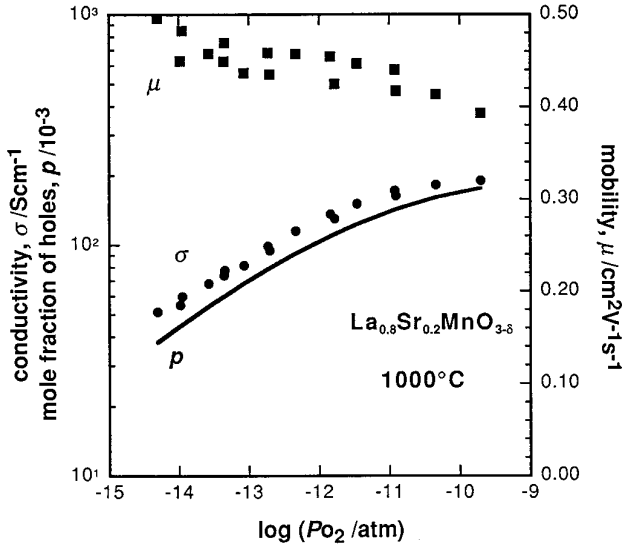

FIG. 9. Oxygen partial pressure dependence of the measured conductivity (σ), hole concentration (p) calculated by using the defect model (MODEL 3), and the hole mobility calculated from σ and p.

holes in the direction opposite to that of oxygen vacancies. This gradient drives the electron holes to counterdiffuse with oxygen vacancies. Thus, the moving species in the process of chemical diffusion in LSM are considered to be electron holes and oxygen vacancies. Assuming that the net current flow along the diffusional direction (perpendicular to the flow of electric current for the conductivity measurement) is zero and that the electronic transference number is unity, the ambipolar diffusion treatment (33) gives the relation (15, 34, 35)

$$\begin{aligned} D_{\text{chem}} &= \frac{D_{\text{h}} D_{\text{V}} (4[\text{V}_{\text{o}}^{\cdot\cdot}] + p)}{4[\text{V}_{\text{O}}^{\cdot\cdot}] D_{\text{V}} + p D_{\text{h}}} \\ &= t_{\text{h}} D_{\text{v}} + t_{\text{i}} D_{\text{h}} \\ &= D_{\text{V}} \left(1 + \frac{4[\text{V}_{\text{O}}^{\cdot\cdot}]}{p}\right), \end{aligned} \qquad [20]$$

where D_{V} and D_{h} are diffusion coefficients of oxygen vacancies and electron holes, t_{i} and t_{h} are ionic and electronic transference numbers, and p is hole concentration. The vacancy diffusion coefficient takes a constant value irrespective of the concentration of vacancy when the interaction between defects is negligible. Here, the enhancement factor of the chemical diffusion coefficient is defined as the ratio of D_{chem} to D_{V}:

$$\text{e.f.} = D_{\text{chem}}/D_{\text{V}}. \qquad [21]$$

Using Eq. [20] in Eq. [21], we get

$$\text{e.f.} = 1 + \frac{4[\text{V}_{\text{O}}^{\cdot\cdot}]}{p}. \qquad [22]$$

The concentrations of oxygen vacancies and electron holes as a function of Po_2 are calculated using MODEL 3, described in the previous section. The equilibrium constants for the defect reactions given in Table 1 are extrapolated to the temperature range in the present investigation using the relation

$$\ln K = -\frac{\Delta S^\circ}{R} + \frac{\Delta H^\circ}{RT}, \qquad [23]$$

where ΔS° and ΔH° are the entropy and enthalpy changes of the respective defect reactions, and are assumed to be temperature independent. The calculated concentrations of oxygen vacancies and electron holes are inserted in Eq. [22] to obtain the enhancement factor. The results are shown in Fig. 10 for the composition with $x = 0.20$ at four different temperatures. It is seen that the enhancement factor decreases with increase of Po_2 and asymptotically approaches unity. The larger enhancement factor at lower Po_2 means that the chemical diffusion coefficient will increase with decrease of Po_2. This theoretical prediction is in good accordance with the experimentally observed Po_2 dependence of D_{chem} previously shown in Figs. 4 and 5. When the above defect chemical analyses are extended into a high Po_2 region ($\log Po_2 > -6$) which is not covered in the present investigation, the chemical diffusion coefficient becomes nearly equal to the vacancy diffusion coefficient since the enhancement factor asymptotically ap-

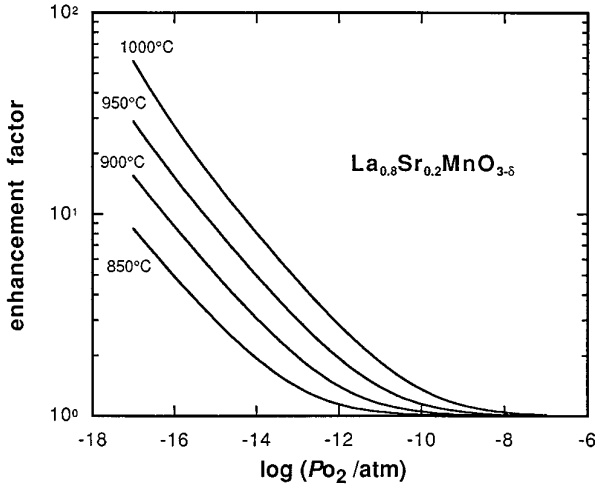

FIG. 10. Enhancement factor of the chemical diffusion coefficient calculated by using Eq. [22].

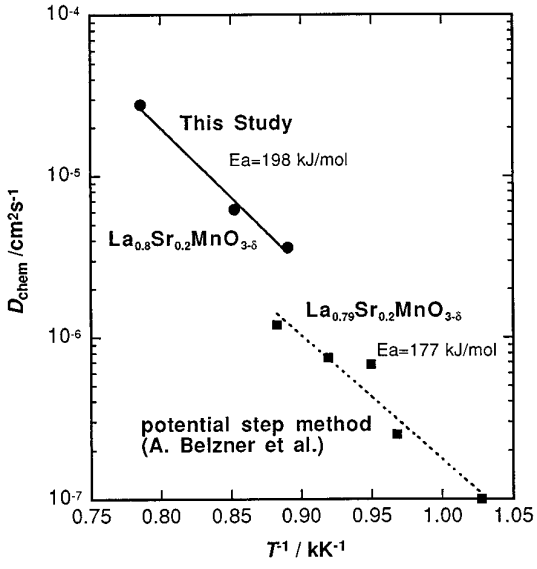

FIG. 11. Temperature dependence of the chemical diffusion coefficient as compared with the literature data of Belzner *et al.* (11). The chemical diffusion coefficient from the present study is extrapolated into the high Po_2 region by approximating the enhancement factor as unity.

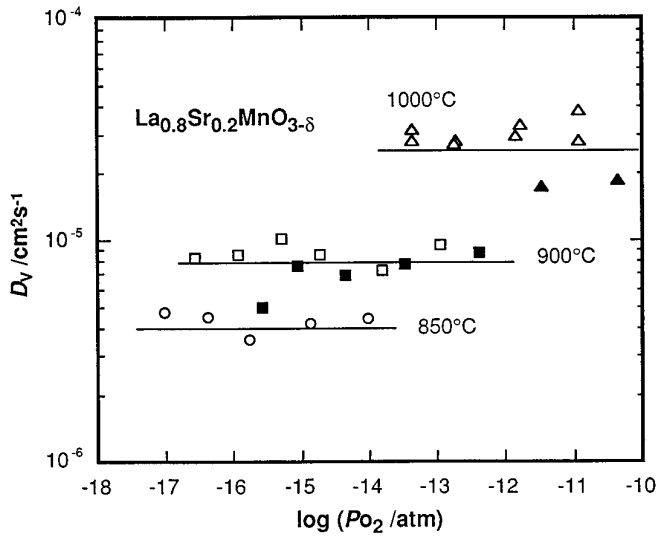

FIG. 12. Oxygen vacancy diffusion coefficient of $La_{0.8}Sr_{0.2}MnO_{3\pm\delta}$ derived from the measured chemical diffusion coefficient by using the defect model (MODEL 3) and the ambipolar diffusion theory. Open and closed symbols are for the results from reduction and oxidation runs, respectively.

proaches unity. In Fig. 11, the D_{chem} thus extrapolated into the high Po_2 region is compared with the data reported by Belzner *et al.* (11), which were obtained by the potential step method at Po_2 of 10^{-8} to 0.21 atm. Although the measurement technique is different and dominant point defects are different under reducing and oxidizing conditions (the predominance of cation vacancies should be considered at high Po_2 as discussed by Kuo *et al.* (20)), the present results agree well with the literature data. This suggests that the chemical diffusion process under high Po_2 conditions is also governed by the ambipolar motion of oxygen vacancies and electron holes.

Using the measured D_{chem} and the calculated enhancement factor in Eq. [22], the vacancy diffusion coefficient can be obtained. Figure 12 shows the Po_2 dependence of D_V derived in this way. It is evident that D_V is independent of Po_2 and hence independent of the vacancy concentration, suggesting that the oxygen vacancies which do not participate in the formation of association pairs behave as free vacancies. The D_V value of 2–3 $\times$ 10^{-5} cm^2 s^{-1} at 1000°C is comparable to those of typical mixed conducting perovskites such as $LaCoO_3$- and $LaFeO_3$-based solid solutions for which fast oxygen diffusion was experimentally demonstrated by Ishigaki *et al.* (36). Therefore, oxygen diffusion in LSM is expected to be quite fast under conditions where LSM show oxygen deficiency. Table 2 lists the numerical values of D_V obtained in the present study.

4.3. Oxygen Partial Pressure Dependence of Surface Reaction Rate Constant

As has already been shown in Fig. 6, the surface reaction rate constant (α) increases with decreased Po_2. This type of Po_2 dependence can be explained by the speculation that the oxygen vacancies present at the surface of LSM play an important role in the surface reaction process: assuming, for example, that the gaseous species (CO and CO_2) involving the surface reaction form a temporary bonding to the vacant lattice sites. The number of oxygen vacancies at the surface increases as Po_2 decreases, which leads to the increase of active sites for the surface reaction and thereby results in larger α.

5. CONCLUSION

The electrical conductivity and chemical diffusion coefficient of $La_{1-x}Sr_xMnO_{3\pm\delta}$ (x = 0.05, 0.10, 0.15, and 0.20) were measured as a function of Po_2. The conductivity

TABLE 2
Oxygen Vacancy Diffusion Coefficient, D_V, of $La_{1-x}Sr_xMnO_{3\pm\delta}$

Composition, x	Temperature [°C]	D_V [cm^2 s^{-1}]
0.05	900	9.67×10^{-6}
0.1	950	4.25×10^{-6}
	1000	3.02×10^{-5}
0.2	850	4.28×10^{-6}
	900	8.06×10^{-6}
	1000	2.79×10^{-5}

relaxation process after a stepwise change of Po_2 in the surrounding atmosphere was successfully interpreted in terms of a diffusion model with consideration of a partial limitation by surface reaction. A defect model considering the formation of association pairs between divalent manganese ions (Mn'_{Mn}) and oxygen vacancies ($V^{\cdot\cdot}_{O}$) was proposed to elucidate the nonstoichiometric behavior of LSM. The model has been shown to satisfactorily explain the Po_2 dependence of oxygen nonstoichiometry, electrical conductivity, and chemical diffusion coefficient. High oxygen vacancy diffusivity was verified from defect chemical analysis of the chemical diffusion data. Oxygen diffusion in LSM will be quite fast under conditions where LSM show oxygen deficiency.

REFERENCES

1. Y. Takeda, R. Kanno, Y. Tomida, and O. Yamamoto, *J. Electrochem. Soc.* **134,** 2656 (1987).
2. K. Tsuneyoshi, K. Mori, A. Sawata, J. Mizusaki, and H. Tagawa, *Solid State Ionics* **35,** 263 (1989).
3. J. Mizusaki, H. Tagawa, K. Tsuneyoshi, and A. Sawata, *J. Electrochem. Soc.* **138,** 1867 (1991).
4. E. Siebert, A. Hammouche, and M. Kleitz, *Electrochim. Acta* **40,** 1741 (1995).
5. A. Hammouche, E. Siebert, A. Hammou, and M. Kleitz, *J. Electrochem. Soc.* **138,** 1212 (1991).
6. M. J. L. Østergård and M. Mogensen, *Electrochim. Acta* **38,** 2015 (1993).
7. A. Momma, Y. Kaga, F. Uchiyama, K. Tsukamoto, and T. Okuo, *in* ''Proceedings, International Fuel Cell Conference, Makuhari, Japan, Feb. 1992.'' NEDO, Tokyo, p. 381.
8. J. Mizusaki and H. Tagawa, *in* ''Proceedings, SOFC-NAGOYA, Nov. 1989'' (O. Yamamoto, M. Dokiya, and H. Tagawa, Eds.), p. 107. Science House Co., Tokyo.
9. J. Mizusaki, H. Tagawa, T. Saito, and H. Narita, *in* ''Proceedings, 14th Risø International Symposium on Materials Science, Roskilde, Denmark, Sept. 1993'' (F. W. Poulsen, J. J. Bentzen, T. Jacobsen, E. Skou, and M. J. L. Østegård, Eds.), p. 343. Risø National Laboratory.
10. T. Ioroi, Y. Uchimoto, Z. Ogumi, and Z. Takehara, *in* ''Proceedings, Fourth International Symposium on Solid Oxide Fuel Cells, Yokohama, June 1995'' (M. Dokiya, O. Yamamoto, H. Tagawa, and S. C. Singhal, Eds.), The Electrochemical Society Proceedings Series, PV 95-1, p. 603. Pennington, NJ.
11. A. Belzner, T. M. Gür, and R. A. Huggins, *Solid State Ionics* **57,** 327 (1992).
12. S. Carter, A. Selcuk, R. J. Charter, K. Kajda, J. A. Kilner, and B. C. H. Steele, *Solid State Ionics* **53–56,** 597 (1992).
13. I. Yasuda and T. Hikita, *in* ''Proceedings, Second International Symposium on Solid Oxide Fuel Cells, Athens, July 1991'' (F. Grosz, P. Zegers, S. C. Singhal, and O. Yamamoto, Eds.), p. 645. Report EUR 13564 EN, Commission of The European Communities.
14. I. Yasuda and T. Hikita, *J. Electrochem. Soc.* **141,** 1268 (1994).
15. I. Yasuda and M. Hishinuma, *J. Solid State Chem.* **115,** 152 (1995).
16. T. Nakamura, G. Petzow, and L. J. Gauckler, *Mater. Res. Bull.* **14,** 649 (1979).
17. Y. Yonemura, H. Nambu, J. Mizusaki, and H. Tagawa, *in* ''Extended Abstracts, First Symposium on Solid Oxide Fuel Cells in Japan, Tokyo, Dec. 1992,'' p. 73. The Solid Oxide Fuel Cells Society of Japan.
18. J. H. Kuo, H. U. Anderson, and D. M. Sparlin, *J. Solid State Chem.* **87,** 55 (1990).
19. J. Crank, *in* ''The Mathematics of Diffusion, 2nd Edition,'' p. 60. Oxford Univ. Press, New York, 1975.
20. J. H. Kuo, H. U. Anderson, and D. M. Sparlin, *J. Solid State Chem.* **83,** 52 (1990).
21. J. Mizusaki, *Solid State Ionics* **52,** 79 (1992).
22. F. A. Kröger, *in* ''The Chemistry of Imperfect Crystals.'' North-Holland, Amsterdam, 1964.
23. B. F. Flandermeyer, M. M. Nasrallah, D. M. Sparlin, and H. U. Anderson, *High Temp. Sci.* **20,** 259 (1985).
24. J. Mizusaki, S. Yamauchi, K. Fueki, and A. Ishikawa, *Solid State Ionics* **12,** 119 (1984).
25. I. Yasuda and T. Hikita, *J. Electrochem. Soc.* **140,** 1699 (1993).
26. R. Raffaelle, H. U. Anderson, D. M. Sparlin, and P. E. Parris, *Phys. Rev. B.* **43,** 7991 (1991).
27. S. E. Dorris and T. O. Mason, *J. Am. Ceram. Soc.* **71,** 379 (1988).
28. J. W. Stevenson, M. M. Nasrallah, H. U. Anderson, and D. M. Sparlin, *J. Solid State Chem.* **102,** 175 (1993).
29. J. Mizusaki, M. Yoshihiro, S. Yamauchi, and K. Fueki, *J. Solid State Chem.* **58,** 257 (1985).
30. J.A.M. van Roosmalen and E. H. P. Cordfunke, *J. Solid State Chem.* **93,** 212 (1991).
31. A. J. Bosman and H. J. val Daal, *Adv. Phys.* **18,** 41 (1970).
32. J. B. Goodenough, *in* ''Progress of Solid State Chemistry, Vol. 5,'' p. 238. (1971).
33. W. van Roosbroeck, *Phys. Rev.* **91,** 282 (1953).
34. J. Schoonman, J. P. Dekker, and J. W. Broers, *Solid State Ionics* **46,** 299 (1991).
35. I. Yasuda and M. Hishinuma, *Solid State Ionics* **80,** 141 (1995).
36. T. Ishigaki, S. Yamauchi, K. Kishio, J. Mizusaki, and K. Fueki, *J. Solid State Chem.* **73,** 179 (1988).